This article has been accepted for publication in a future issue of this journal, but has not been fully edited. Content may change prior to final publication. Citation information: DOI 10.1109/TGRS.2022.3165001, IEEE Transactions on Geoscience and Remote Sensing

An Improved Blackbody Calibration Cadence for CYGNSS

C. E. Powell, *Student Member, IEEE*, Christopher S. Ruf, *Fellow, IEEE*, and Anthony Russel

***Abstract*— An improved blackbody calibration procedure is developed, implemented, and tested for the Cyclone Global Navigation Satellite System (CYGNSS). Previously, CYGNSS calibrated its receivers once every minute to account for temperature-induced gain fluctuations. The time spent making calibration measurements limited the duty cycle of windspeed measurements to approximately 90%. Analysis presented here shows that the one-minute cadence was overly conservative and can be increased to once every 10 minutes with minimal impact to data quality, thereby improving the windspeed duty cycle to 98%. A permanent change to the blackbody cadence was made for the complete 8 satellite constellation during July 27, 2021 – August 3, 2021, and subsequent analysis verifies that the new cadence improves duty cycle without impacting science data quality, as expected.**

***Index Terms*—Cyclone Global Navigation Satellite System (CYGNSS), Global Navigation Satellite System-Reflectometry (GNSS-R), calibration, blackbody, remote sensing.**

I. INTRODUCTION

LAUNCHED in 2016, NASA's Cyclone Global Navigation Satellite System (CYGNSS) mission has been collecting global observations between +/- 38 degrees latitude with a technique known as global navigation satellite system (GNSS) reflectometry [1]. CYGNSS works by measuring the reflections of GNSS signals from Earth's surface, in effect operating as an opportunistic bistatic radar. Designed to investigate the evolution and structure of tropical cyclones, CYGNSS is comprised of eight microsatellites in equatorial low Earth orbit [2]. With this architecture, CYGNSS measures the reflected power of GNSS signals from Earth's surface with fast revisit time (2.8 hour median, 7.2 hour mean) that allows for rapid acquisition of dynamic weather events [3].

CYGNSS's utility is impaired by a suboptimal sampling cadence related to the satellite's onboard calibration system. The sequencing rate for sampling the onboard blackbody calibration target had been once every minute since launch, and each time this event occurred, the calibration would last approximately four seconds, inclusive of the time required to switch loads from the antenna source to the onboard blackbody target. As a result, CYGNSS occasionally missed sampling certain high-value targets.

Based on the analysis presented below, the flight software was updated in 2021 to modify the sampling cadence to once every 10 minutes, with a slightly increased dwell time of approximately six seconds. This improves the windspeed retrieval duty cycle from 90% to 98% and shows no detectable deterioration in performance.

II. THEORY

CYGNSS measures ocean surface roughness as a proxy for ocean surface windspeed. Mean ocean surface roughness is estimated from the normalized bistatic radar cross section (NBRCS) measured at L-band (1575 MHz). The NBRCS is determined from the scattered power received at the CYGNSS satellite by [4]

$$\sigma^o = \frac{P_g (4\pi)^3 L I (R^T R^R)^2}{P^T G^T \lambda^2 G^R A} \tag{1}$$

where σ^o is NBRCS, P_g is the received power; L is the atmospheric attenuation along the propagation path from the GPS satellite to the specular point and to CYGNSS; I is a term to account for instrument losses, R^T and R^R are the ranges between the specular point and the transmitter and CYGNSS receiver, respectively; P^T is the transmit power of the GPS satellite; G^T is the antenna gain of the GPS satellite in the direction of the specular point; λ is the wavelength of the GPS L1 signal; G^R is the gain of the CYGNSS nadir receive antenna in the direction of the specular point; and A is the effective scattering area. Note that P_g and A vary as functions of the time delay and Doppler shift of the received signal. As a result, NBRCS also depends on delay and Doppler. The NBRCS determined at all sampled values of delay and Doppler is referred to as a Delay Doppler Map (DDM).

NBRCS is directly related to the mean square slope (MSS) of ocean wave spectra via [5], [6]

$$\sigma^o(\theta) = \frac{|\Re(\theta)|^2}{MSS} \tag{2}$$

This work was supported in part by the National Aeronautics and Space Administration Science Mission Directorate contract NNL13AQ00C with the University of Michigan. *(Corresponding author: C. E. Powell)*

C. E. Powell is with the Department of Climate and Space Sciences and Engineering, University of Michigan, Ann Arbor, MI 48109 USA (email: cepowell@umich.edu).

Christopher S. Ruf is with the Department of Climate and Space Sciences and Engineering, University of Michigan, Ann arbor, MI 48109 USA, and also with the Department of Electrical Engineering and Computer Science, University of Michigan, Ann Arbor, MI 48109 USA (email: cruf@umich.edu).

Anthony Russel is with the Space Physics Research Laboratory, University of Michigan, Ann Arbor, MI 48109 USA (email: russelan@umich.edu).

Color versions of one or more of the figures in this article are available online at http://ieeexplore.ieee.org

This article has been accepted for publication in a future issue of this journal, but has not been fully edited. Content may change prior to final publication. Citation information: DOI 10.1109/TGRS.2022.3165001, IEEE Transactions on Geoscience and Remote Sensing

where θ is the angle of incidence of the scattering geometry and $\Re(\theta)$ is the Fresnel reflection coefficient for the ocean surface at the specular point.

Stronger received signals P_g indicate smoother, more specular scattering of the ocean surface; weaker signals indicate rougher ocean surfaces associated with higher windspeed. CYGNSS's electronics measures received power in raw digital counts, and calibrated received signal power P_g in units of Watts is calculated by

$$P_g = \frac{C - C_N}{G} \tag{3}$$

where G is receiver gain in Watts/count, C is the raw counts measured at delay-Doppler bins where a scattered signal is present, and C_N is the mean raw counts for background noise without any scattered signal present. In practice, C_N is an average over many delay-Doppler bins at delay coordinates shorter than that of the specular point. Shorter delays correspond to radar reflections from the atmosphere above the ocean surface, for which there is no appreciable scattering at L-Band.

CYGNSS satellites are in an equatorial low-Earth orbit with a period of approximately 95 minutes, and experience significant variations in their thermal loads associated with their orbit. As each satellite crosses the terminator into sunlight, the body heats unevenly, causing thermal gradients across the structure. As the spacecraft enters the nightside, it cools suddenly and unevenly.

As the body of the structure changes temperature, so does the thermal environment of the CYGNSS receiver electronics. These dynamics induce variations in the gain of CYGNSS's receiver. Because the quality of windspeed retrieval depends on the consistency of receiver power, each satellite's nadir instruments have built-in onboard calibration equipment to account for thermal gain variations in the receiver amplifiers.

CYGNSS has two nadir science antennas, facing the satellite's port and starboard directions, respectively. The receiver connected to each nadir science antenna has its own blackbody calibration target. A thermistor adjacent to the target monitors its temperature in real time to determine the power in the blackbody thermal emission. During a blackbody calibration sequence, the input to the receiver is redirected from the science antenna to the blackbody load and the power emitted by the blackbody is recorded in raw counts for later processing. This sequence takes approximately four seconds because the calibration clock and the science data clock are not synchronized, and the switching of loads is not perfectly instantaneous. To ensure that a full reading of the blackbody is measured without contamination from the load switching process, samples immediately preceding and succeeding calibration are flagged out.

During data processing, the nearest calibration samples before and after a science sample are linearly interpolated to the time of the science sample to estimate gain variations between calibration looks. At launch, this sequence was scheduled to occur once every minute, such that every science sample was within approximately 30 seconds of a receiver calibration event. This calibration sequence sets receiver gain for calculating received power as given by

$$G = \frac{C_B}{P_B + P_r} \tag{4}$$

where C_B is the counts measured while looking at the blackbody load, P_B is the power from the blackbody as estimated from the thermocouple on the low noise amplifier, and P_r is the receiver noise estimated from a temperature-dependent noise floor parameterization determined pre-launch. All three values vary as the spacecraft temperature fluctuates. The one-minute cadence was estimated to bound the 1-sigma calibration error for the received power to 0.13 dB [7].

Fig. 1 shows how the spacecraft gain varies with temperature. The blue trace is the calibrated receiver gain in dB, the red trace is variation in low-noise amplifier temperature in degrees Celsius. The gain varies approximately 0.4-0.6 dB peak-to-peak, whereas the absolute temperature of the low-noise amplifier varies approximately 8 degrees Celsius peak-to-peak.

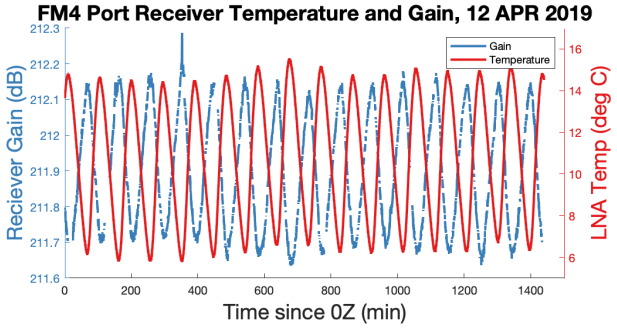

Fig. 1. Example of temperature influence on receiver gain. Above, FM4's port receiver gain is plotted (blue) with the temperature at a nearby probe (red) for a full day starting at 0Z 12 APR 2019. Note that gain is inversely related to local temperature, and that these swings are periodic, consistent with CYGNSS's 95-minute orbital period.

CYGNSS's thermal environment also varies due to the orientation of its orbit plane relative to the sun. The relative time spent in sunlight or shade varies throughout the year as the orbital plane precesses about the Earth. This precession is conveniently characterized by the time dependent nature of the angle between the orbit plane and a line from the Earth to the sun, referred to as the orbit beta angle (see Fig. 2). In general, CYGNSS is exposed to the greatest temperature variations during low magnitudes of orbit beta angle, which implies that the spacecraft will spend the maximum amount of time in shade [8]. Additionally, during periods at the highest beta angles, at approximately 50 degrees in magnitude and greater, the spacecraft are commanded into a roll configuration to maintain adequate solar radiance on the solar array panels.

This article has been accepted for publication in a future issue of this journal, but has not been fully edited. Content may change prior to final publication. Citation information: DOI 10.1109/TGRS.2022.3165001, IEEE Transactions on Geoscience and Remote Sensing

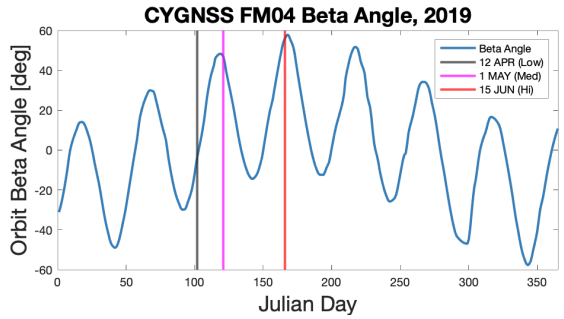

Fig. 2. Orbit beta angle calculated for FM04 for 2019. The black, magenta, and orange vertical lines denote the low, medium, and high beta angle days respectively.

III. Methods

Decreasing the calibration frequency risks increasing error caused by inaccurate compensation for time-varying receiver gain. Science data taken between blackbody calibration measurements are calibrated using linearly interpolated values of the nearest calibration data before and after the science measurement. If the temperature of the spacecraft receiver electronics changes in a non-linear way between calibrations, it can result in significant errors due to improper corrections for gain variation. An on-orbit experiment was performed to explore how two fundamental CYGNSS data products, NBRCS and retrieved windspeed, degrade due to an increase in the time between blackbody samples.

Three days of data from one satellite (FM4) were used, with days selected representing different characteristic beta angles to explore how different thermal cycling may impact the calibration sequence, as shown in Table I.

TABLE I

ESTIMATED BETA ANGLE AND THERMAL VARIATION FOR SELECTED DAYS

Date	Orbit Beta Angle	Peak-to-peak Temperature Swing
12 APR 2019	-3 deg ("Low")	9.8 deg C
1 MAY 2019	46 deg ("Med')	6.6 deg C
15 JUN 2019	56 deg ("High")	5.6 deg C

For all three days, science samples were collected and processed with normal one-minute blackbody sampling. This generated baseline measurements: the fully-developed sea (FDS) windspeed retrieval product u_{FDS_1}, the young-seas limited-fetch (YSLF) windspeed retrieval product u_{YSLF_1}, and the NBRCS σ_1^o [9]. CYGNSS uses two separate geophysical model functions for windspeed retrieval. Both retrievals are empirical fittings, but the YSLF differs from the FDS in its sensitivity to longwave swell, which tends to be under-developed in high-wind, dynamic weather where wind direction is frequently changing, such as during tropical cyclones [10], [11]. The YSLF product is tuned to respond to higher wind speed conditions where measurement sensitivity is diminished, and so will be more sensitive to possible degradation in calibration quality that results from the change in blackbody cadence.

These data were then reprocessed using every *n*th blackbody sample, where *n* is an integer that ranged from 2 through 45, representing sampling the blackbody once every *n* minutes. The maximum value considered corresponds to performing a blackbody calibration approximately once every half orbit. Between the blackbody samples used, the raw counts recorded by the blackbody were linearly interpolated. An additional case was considered in which the daily mean value of all blackbody samples was used to calibrate the entire day of science data. This case represents calibration without regard for short term gain variations.

Degradation in calibration accuracy is assessed by examining the difference between science samples calibrated using every nth blackbody sample vs. using blackbody samples every minute. These differences are given by

$$\Delta u_n = u_n - u_1 \tag{5}$$

where u_n is the windspeed produced at a calibration period of n minutes, u_1 is the windspeed produced at the original calibration sequence, and Δu_n is the difference in windspeed due to increased calibration period of n minutes. If u_1 is assumed to be accurately calibrated, Δu represents the error that results from less-frequent blackbody calibration. Similar values can be produced for NBRCS and gain:

$$\Delta\sigma_n^o = \sigma_n^o - \sigma_1^o \tag{6}$$
$$\Delta G_n = G_n - G_1 \tag{7}$$

where σ_n^o is the NBRCS at n-minute calibrations, σ_1^o is the NBRCS produced during one-minute calibrations, and $\Delta\sigma_n^o$ is the NBRCS error induced by sampling at longer periods; and G_n is the receiver gain at n-minute calibrations, G_1 is the original gain at one minute sampling, and ΔG_n is the error due to a longer calibration sequence at period n.

If the use of a particular (longer) sampling rate produces a measurable change in the derived CYGNSS data products relative to the 1-minute baseline measurements, that is an indication of a degradation in calibration accuracy.

To explore a "worst case" scenario, an additional comparison is made assuming the satellite only calibrates the blackbody once per day using the daily average value. This provides a sense for how NBRCS and windspeed would degrade if the calibration was performed at timescales much slower than the orbit-induced changes in the thermal loading of the spacecraft.

A. Characterizing the Impact of Change in Cadence

Changing the period of calibration impacts the quality of the gain estimate in (4). If the non-linear component of the thermal environment changes at timescales faster than the calibration period, the gain estimated by the calibration process will no longer be representative of the true gain.

Fig. 3 depicts histograms of normalized gain changes due to increased blackbody sampling cadences. For every sample, both the original gain and the relative fraction of its change is calculated. At blackbody sampling rates close to one minute, there is very little difference from the original gain, and distribution of samples approach a delta function. At longer

This article has been accepted for publication in a future issue of this journal, but has not been fully edited. Content may change prior to final publication. Citation information: DOI 10.1109/TGRS.2022.3165001, IEEE Transactions on Geoscience and Remote Sensing

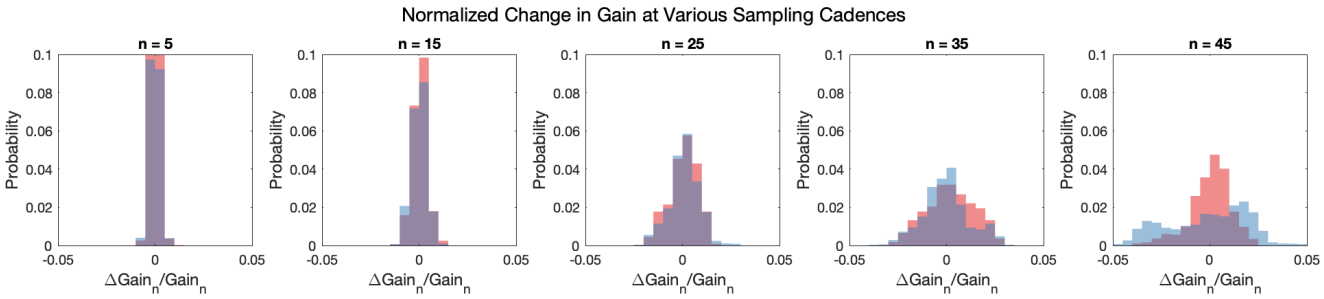

Fig. 3. Histograms of gain error at n = {5, 15, 25, 35, 45} minutes. The blue and red distributions represent data from the port and starboard antennas, respectively. At low *n*, the gain error approaches a delta function. As sampling cadence time increases, the distribution widens, illustrating the degradation from the original one-minute sampling cadence.

sampling intervals, this distribution widens, illustrating how gain estimates degrade as the sampling cadence increases. At approximately two samples per orbit, or n = 45, the gain variations can be up to +/- 5% of the baseline.

The results in Fig. 3 are shown for the impact on gain, but this behavior is observed across all derived products. To estimate the growth in error as a function of sampling cadence, the standard deviation is calculated for each distribution. Fig. 4 shows how the standard deviation grows as the sampling period increases.

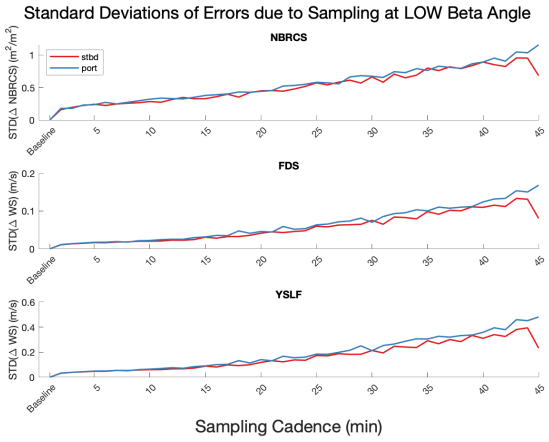

Fig. 4. Standard deviations of growth in error as a function of sampling cadence for NBRCS (top), FDS windspeed (middle), and YSLF windspeed (bottom) at low beta angle. Red traces indicate values for the starboard antenna, and blue traces for the port side.

Sampling every 2 minutes, the NBRCS error standard deviation is approximately 0.25 m2/m2. This grows to an error of just over 1 m2/m2 at 45 min cadence. The error characteristics for sampling once per day resembles the 45-minute scenario, as the sampling at every half-orbit maximizes error due to unrepresentative temperature-dependent gain corrections. The standard deviation of windspeed error is approximately three times larger for the YSLF retrieval than the FDS retrieval. At the worst possible case, sampling once every day, the standard deviation of error on the windspeed product approaches 0.6 m/s. For context, the requirement for CYGNSS retrieval accuracy is a root-mean-square (RMS) error of less than 2 m/s at windspeeds lower than 20 m/s, and RMS error of less than 10% at winds greater than 20 m/s [6]. The error inventory for the mission suggests that the total L1 error will be 0.82 dB at low wind speeds and 0.70 dB at high winds [4]. Assuming a low wind NBRCS of 100 and a high wind NBRCS of 16, the once-daily sampling degrades the measurement by 0.04 dB and 0.28 dB respectively. Therefore, even at this cadence, the magnitude of the standard deviation of error is still small enough to meet system requirements.

The standard deviation can, however, be a misleading metric, as it describes the behavior of the total distribution, as opposed to errors in high-value samples. Changes in NBRCS are much more significant at low values, because NBRCS is inversely related to windspeed. In addition, large errors in windspeed retrievals in high-wind areas such as hurricanes can be averaged out by the much more frequent and smaller errors over calm seas.

For this reason, a new metric is developed to appropriately capture how modifications in calibration cadence can impact the CYGNSS science products. This metric is named PCT1, which stands for the percent of samples with error magnitudes that are 1% or greater than its value when using the original

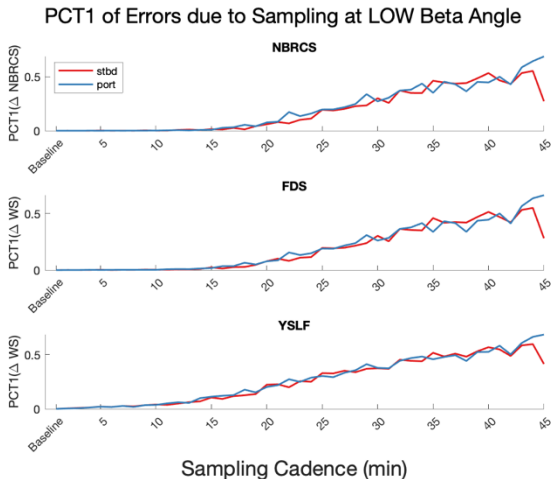

Fig. 5. PCT1 of error as a function of sampling cadence period for NBRCS (top), FDS windspeed (middle), and YSLF windspeed (bottom) at low beta angle. Red traces indicate values for the starboard antenna, and blue traces for the port side.

This article has been accepted for publication in a future issue of this journal, but has not been fully edited. Content may change prior to final publication. Citation information: DOI 10.1109/TGRS.2022.3165001, IEEE Transactions on Geoscience and Remote Sensing

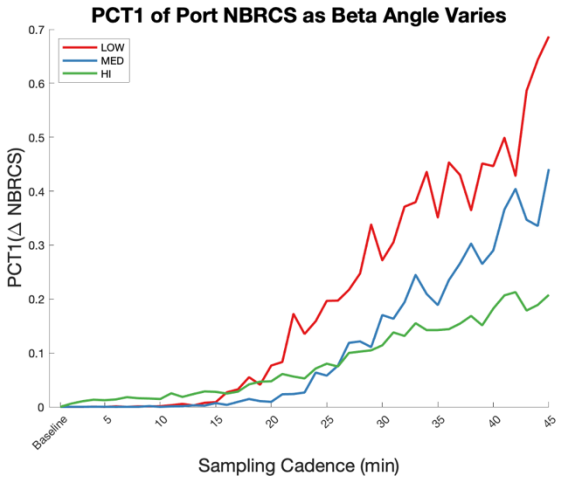

Fig. 6. PCT1 of NBRCS error as a function of sampling cadence period at various beta angles. At lower beta, the performance degradation is more pronounced.

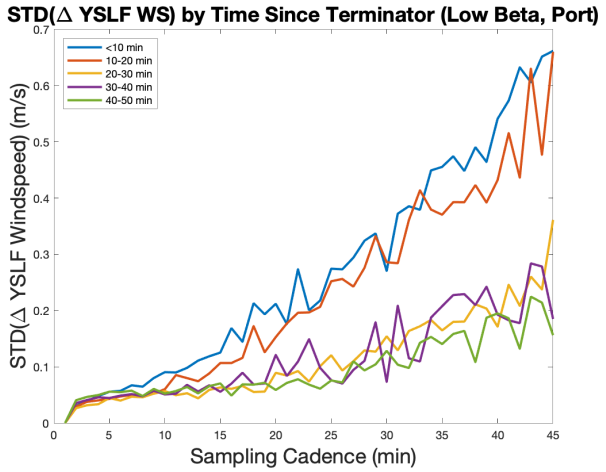

Fig. 7. Standard deviation of YSLF windspeed error as a function of sampling cadence period at various orbit sectors. The errors due to increased blackbody sampling rates are greatest immediately after crossing the terminator. This effect is largest at longer sampling periods.

one-minute calibration cadence. The PCT1 metric ranges from 0 to 1, with 0 indicating that no samples have errors greater than 1%, and 1 indicating that every sample has an error which is at least 1%. The PCT1 for the 3 data products is shown in Fig. 5. As the cadence period increases, the PCT1 rises, with an inflection point between 10 and 15 minutes. At that point, the increase in blackbody cadence significantly impacts the overall population of data. As expected, the YSLF windspeed retrieval is the most sensitive product to changes in the blackbody sampling rate.

To see how this relationship varies across different orbit beta angles and resulting thermal conditions, the PCT1 for NBRCS is plotted across different orbit beta angles in Figure 6. At lower beta angles, the errors are more pronounced, as the spacecraft spends more time in the shaded portion of the orbit, resulting in greater temperature variability.

B. Optimal Blackbody Sampling Cadence

Determining an optimal sampling cadence requires exploring the tradeoff between the potential benefit of increased science duty cycle over the cost of potentially poorer instrument performance.

For this analysis, the worst possible conditions are employed to provide an upper bound on potential impacts to downstream products. Because the low beta angle orbit has greatest temperature variability, it leads to increased performance degradation, and because the YSLF windspeed product is more sensitive to calibration errors than its FDS counterpart, the choice of blackbody sampling rate should be driven by the low beta YSLF error growth.

We chose an arbitrary YSLF PCT1 value of 0.05 as the optimal cutoff threshold, which means that the number of samples with greater than 1% error due to increased sampling period could be no more than 5% of the total population. The largest sampling rate below the PCT1 cut-off for the YSLF data product is once every 10 minutes as shown in Fig. 5. At 11 minutes, the PCT1 values exceed 0.05 during the low beta angle day.

IV. Performance by Orbit Sector

The temperature gradients on CYGNSS are the largest as the spacecraft crosses the terminator. This implies that the performance degradation due to increased sampling period should be greatest as the spacecraft crosses the terminator. To validate this theory, we calculate the standard deviation of the windspeed anomaly as a function of sampling cadence as before, and further segregate results by orbital phase.

The terminator crossing is approximated by utilizing the temperature traces of the low-noise amplifiers. The spacecraft is assumed to cross the terminator five minutes prior to each peak and valley of the temperature trace. After the terminator crossings are established, the time since crossing the terminator is segregated into five 10-minute bins.

Fig. 7 shows the standard deviation of the YSLF windspeed anomaly for the low beta case, separated by time since terminator crossing. The performance impact of increasing the sampling cadence is clearly dependent on orbital location, with the worst performance immediately following the terminator crossing, and moderate impacts as the spacecraft enters a steady-state thermal environment.

V. Discussion

As a result of this analysis, the CYGNSS operations team elected to transition science operations to the 10-minute blackbody sampling cadence in August 2021.

A. Characterizing the Impact to Duty Cycle

To evaluate the utility of a refined sampling cadence, the preferred figure of merit is the duty cycle of high-quality ocean observations in which windspeed retrievals are possible, as given by

$$D_{fom} = \frac{N_{good}}{N_{good} + N_{BB}} \tag{8}$$

This article has been accepted for publication in a future issue of this journal, but has not been fully edited. Content may change prior to final publication. Citation information: DOI 10.1109/TGRS.2022.3165001, IEEE Transactions on Geoscience and Remote Sensing

where N_{good} is the number of good-quality ocean observations capable of otherwise retrieving a windspeed retrieval, and N_{BB} is the number of samples impacted by the blackbody calibration sequence.

The original 1-minute blackbody cadence took on average four seconds, inclusive of the time it took for the spacecraft to switch loads (1 s), sample the blackbody target (2 s), and switch back to the science antenna (1 s). This would suggest a nominal duty cycle of approximately 56/60 = 93.33% as computed in (8) without considering other factors.

For the 10-minute sequence, the length of time observing the blackbody target was increased to four seconds to reduce variability due to sudden receiver excursions. When considering the two seconds required for changing the antenna load to the target, an average blackbody measurement takes approximately six seconds. Theoretically, the duty cycle should improve to 594/600 = 99%.

CYGNSS L1 data files have several quality flags associated with each sample, and N_{good} is determined by an "overall quality" indicator, which is the sum of several other flags with logical OR operations as described in the product data dictionary [12]. In practice, only about 60% of samples collected over the ocean are useful due to other quality control flags independent of the blackbody calibration. Therefore, any improvement in the raw duty cycle with a new blackbody sequence will have outsized impact in D_{fom}. When accounting for this difference, the expected D_{fom} in the naïve 1-minute cadence where 6.67% data are lost is no longer 93%, but approximately 89% as 6.67% / 0.6 = 11%. Similarly, the expected D_{fom} for the improved blackbody sequence is 98%.

N_{BB} is composed of logical ORs of flags associated with the blackbody sample itself plus flags that indicate the instrument is reconfiguring in preparation for or immediately after a blackbody sample, adjusted for samples that occur only over the ocean. By implementing this modification, the D_{fom} increases from approximately 90% to 98%.

B. Characterizing the Impact to the Level 1A Error Budget

CYGNSS's Level 1 error budget described in the Algorithm Theoretical Basis Document is composed of the root sum of squares of individual error terms in the Level 1A equation [13]. Combining (3) and (4) shows the full Level 1A equation with each source term

$$P_g = \frac{(C - C_N)(P_r + P_B)}{C_B} \tag{9}$$

The individual error terms can be approximated by taking the partial derivative with respect to each individual term

$$E(q_i) = \left|\frac{\partial P_g}{\partial q_i}\right| \Delta q_i \tag{10}$$

where q_i represents an individual input parameter. The total error from the root sum of squares of individual error terms can be expressed as

$$E_{L1A} = \left[\sum_i [E(q_i)]^2\right]^{\frac{1}{2}} \tag{11}$$

In this experiment, we modified the input parameter C_B and held all other inputs constant. Therefore, we can calculate the specific contribution of error due to the blackbody sequence by plugging (9) into (10) and setting $q_i = C_B$:

$$E(C_B) = \frac{(C - C_N)(P_r + P_B)}{C_B^2} \Delta C_B \tag{12}$$

The latest Level 1A error budget estimates that the 1-sigma $E(C_B)$ is 0.05 dB [7]. With the change in blackbody cadence from 1 minute to 10 minutes, the one-sigma uncertainty becomes approximately 0.07 dB. The total error now follows by computing the root sum of squares in (11) with the other values specified in Gleason et. al (2019) [7]. Prior to the blackbody calibration, the rolled-up Level 1A error budget was 0.225 dB, and after the change, it has increased to 0.232 dB.

C. Comparing Expected Results to Empirical Data

To demonstrate that windspeed performance has not significantly deteriorated, a statistical comparison is performed with reanalysis data using the CYGNSS Climate Data Record Version 1.1. This product matches up MERRA-2 windspeed reanalysis with CYGNSS observations, and generates an expected "modeled" NBRCS for a given ocean condition with the appropriate spectral corrections for CYGNSS. The performance of the CYGNSS retrieval is compared as the difference in measured NBRCS versus modeled NBRCS for each sample before and after the calibration sequence:

$$(\Delta\sigma^o)_{1\,min} = (\sigma^o_{obs} - \sigma^o_{mod})_{1\,min} \tag{13a}$$

$$(\Delta\sigma^o)_{10\,min} = (\sigma^o_{obs} - \sigma^o_{mod})_{10\,min} \tag{13b}$$

To account for variability in global windspeed distributions, 24 prior samples at the 1-minute cadence were selected in 2020 to account for any seasonal or sub seasonal variability in CYGNSS performance. Because year-round data is not available for the new sampling cadence, a week of data was collected to represent current behavior.

With this data, Student's T-test was performed with both the standard deviation and mean of $\Delta\sigma^o$ to evaluate if there were any statistically significant changes in the performance of CYGNSS. Each day of the 1-minute data serves as a realization of the prior distribution, and the week of 10-minute data is a realization used in the significance test, where the parameters are shown in (14a-d). To minimize the sensitivity to outliers, only values between the 5th and 95th percentiles of each dataset were utilized.

$$\mu_1 = mean(\Delta\sigma^o)_{1\,min}\,;\ \mu_2 = mean(\Delta\sigma^o)_{10\,min} \tag{14a}$$

$$s_1 = std(\Delta\sigma^o)_{1\,min}\,;\ s_2 = std(\Delta\sigma^o)_{10\,min} \tag{14b}$$

$$H_0: \mu_1 = \mu_2, H_1: \mu_1 \neq \mu_2 \quad (14c)$$

$$H_0: s_1 = s_2, H_1: s_1 \neq s_2; \quad (14d)$$

TABLE II

SUMMARY OF CYGNSS PERFORMANCE BEFORE AND AFTER BLACKBODY SEQUENCE MODIFICATION

Parameter	Confidence interval of 1-minute cadence	Value at 10-minute cadence	Significance (p-value)
mean($\Delta\sigma^o$)	11.91 - 51.92	14.77	0.3866
std($\Delta\sigma^o$)	53.56 - 61.59	54.87	0.1755

As shown in Table 2, there are no statistically significant differences in the overall performance of CYGNSS, both in terms of the average absolute performance of the difference between observations and expected NBRCS values, as well as any appreciable increase in variability. The errors inherent in windspeed model performance are several orders of magnitude greater than any expected deterioration that could be attributed to elongated blackbody sequence.

VI. SUMMARY AND CONCLUSIONS

This work explores an optimal blackbody sampling cadence for the CYGNSS constellation. Fundamentally, the calculus to modify sampling cadence weighs the potential deterioration of data quality as a result of less precise thermal gain variation knowledge against the potential utility of increased science collection coverage.

With this analysis, we show that the original design generally overestimated the effects of thermal gain variations on the end derived products and the calibration sequencing oversampled at the expense of science operations.

The most dynamic thermal environment for CYGNSS spacecraft occurs as they cross the terminator, and the most significant variations occur when the orbit is at its lowest beta angle, when the spacecraft has the longest opportunity to cool in Earth's shadow. Under those conditions, any changes to the blackbody cadence will have the most significant impact on the derived products. However, even considering CYGNSS's most sensitive product, the YSLF windspeed, the blackbody sampling rate can be increased 10-fold to once every 10 minutes without degrading more than 5% of the data population by more than 1%.

With this modification, CYGNSS is able to improve its retrieval duty cycle from 90% to 98%, significantly improving the availability of data previously lost to excessive blackbody calibration.

REFERENCES

[1] C. Ruf *et al.*, "In-Orbit Performance of the Constellation of CYGNSS Hurricane Satellites," *Bull. Am. Meteorol. Soc.*, Jun. 2019.

[2] C. Ruf *et al.*, "CYGNSS: Enabling the Future of Hurricane Prediction [Remote Sensing Satellites]," *IEEE Geosci. Remote Sens. Mag.*, vol. 1, no. 2, pp. 52–67, Jul. 2013.

[3] C. Ruf, S. Gleason, A. Ridley, R. Rose, and J. Scherrer, "The nasa cygnss mission: Overview and status update," *Int. Geosci. Remote Sens. Symp.*, vol. 2017-July, pp. 2641–2643, 2017.

[4] S. Gleason, C. S. Ruf, M. P. Clarizia, and A. J. O'Brien, "Calibration and unwrapping of the normalized scattering cross section for the cyclone global navigation satellite system," *IEEE Trans. Geosci. Remote Sens.*, vol. 54, no. 5, pp. 2495–2509, May 2016.

[5] C. Ruf *et al.*, *CYGNSS Handbook - Cyclone Global Navigation Satellite System*. NASA, 2016.

[6] M. P. Clarizia and C. S. Ruf, "Wind Speed Retrieval Algorithm for the Cyclone Global Navigation Satellite System (CYGNSS) Mission," *IEEE Trans. Geosci. Remote Sens.*, vol. 54, no. 8, pp. 4419–4432, Aug. 2016.

[7] S. Gleason, C. S. Ruf, A. J. Orbrien, and D. S. McKague, "The CYGNSS Level 1 Calibration Algorithm and Error Analysis Based on On-Orbit Measurements," *IEEE J. Sel. Top. Appl. Earth Obs. Remote Sens.*, vol. 12, no. 1, pp. 37–49, Jan. 2019.

[8] J. P. Grey, I. R. Mann, M. D. Fleischauer, and D. G. Elliott, "Analytic model for low earth orbit satellite solar power," *IEEE Trans. Aerosp. Electron. Syst.*, vol. 56, no. 5, pp. 3349–3359, Oct. 2020.

[9] CYGNSS, "CYGNSS Level 2 Science Data Record Version 3.0," *2020*. [Online]. Available: doi:10.5067/CYGNS-L2X30.

[10] C. S. Ruf and R. Balasubramaniam, "Development of the CYGNSS Geophysical Model Function for Wind Speed," *IEEE J. Sel. Top. Appl. Earth Obs. Remote Sens.*, vol. 12, no. 1, pp. 66–77, Jan. 2019.

[11] C. S. Ruf, S. Gleason, and D. S. McKague, "Assessment of CYGNSS Wind Speed Retrieval Uncertainty," *IEEE J. Sel. Top. Appl. Earth Obs. Remote Sens.*, vol. 12, no. 1, pp. 87–97, Jan. 2019.

[12] CYGNSS, "CYGNSS Level 1 Science Data Record Version 3.0," *PO.DAAC*, 2020. [Online]. Available: doi:10.5067/CYGNS-L1X30.

[13] S. Gleason, "Cyclone Global Navigation Satellite System (CYGNSS) Algorithm Theoretical Basis Document Level 1A DDM Calibration," 2014.

Acknowledgement. The authors thank the two anonymous reviewers for their helpful comments and feedback.

C. E. Powell (Student Member, IEEE) received the Sc.B. degree in physics from Brown University, Providence, RI, USA, in 2013, the M.A. degree in Russian, East European, and Eurasian studies from Stanford University, Stanford, CA, USA, in 2014, and the M.S. degree in climate and space sciences and engineering from the University of Michigan, Ann Arbor, MI, USA, in 2021.

Since 2016, he has worked at the National Oceanic and Atmospheric Administration (NOAA), Silver Spring, MD, USA, in a variety of policy and programmatic capacities supporting national environmental observation and prediction requirements. He is currently a doctoral candidate at the University of Michigan, Ann Arbor, MI, USA, where he investigates novel remote sensing techniques.

Mr. Powell is a member of the American Meteorological Society (AMS) and American Geophysical Union (AGU).

Christopher S. Ruf (Fellow, IEEE) received the B.A. degree in physics from Reed College, Portland, OR, USA, in 1982, and the Ph.D. degree in electrical engineering and computer engineering from the University of Massachusetts at Amherst, Amherst, MA, USA, in 1987.

He has worked previously at Intel Corporation, Aloha, OR, USA, Hughes Space and Communication, El Segundo, CA, USA, the NASA Jet Propulsion Laboratory, Pasadena, CA, USA, and Pennsylvania State University, University Park, PA, USA. He is the Frederick Bartman Collegiate Professor of climate and space science with the University of Michigan, Ann Arbor, MI, USA, and Principal Investigator of the NASA Cyclone Global Navigation Satellite System mission. His research includes GNSS-R remote sensing, microwave radiometry, atmosphere and ocean geophysical retrieval algorithm development, and sensor technology development.

Dr. Ruf is a member of the American Geophysical Union (AGU), the American Meteorological Society (AMS), and Commission F of the Union Radio Scientifique Internationale. He is a former Editor-in-Chief of the IEEE Transactions on Geoscience and Remote Sensing and has served on the editorial boards of Radio Science and the Journal of Atmospheric and Oceanic Technology. He is the recipient of four NASA Certificates of Recognition and seven NASA Group Achievement Awards, as well as the 1997 TGRS Best Paper Award, the 1999 IEEE Resnik Technical Field Award, the 2006 IGARSS Best Paper Award, and the 2014 IEEE GRSS Outstanding Service Award.

Anthony Russel received the B.S. degree in computer science engineering from Michigan State University, East Lansing, MI, USA in 2014.

He is a member of the engineering staff with the Space Physics Research Laboratory, College of Engineering, University of Michigan, Ann Arbor, MI, USA. His primary engineering activities involve algorithm development and large-scale data processing as a member of the Science Operation Center for the CYGNSS mission.